opposed to 19,000 to 23,000 years in the insolation record), indicating a more complicated relation (*15, 16*).

Our results demonstrate that embedded within the long-term climatic changes were much finer scale variations at sub-Milankovitch time scales (Fig. 2). We therefore propose that, in addition to the climatic changes associated with the linear response to the orbital forcing, a nonlinear response at sub-Milankovitch frequencies may have been responsible for the initiation of the NHG. Perhaps an incremental increase in amplitude and frequency of these sub-Milankovitch oscillations across the transition resulted in a shortening of the length of time between subsequent cold stages. This would have reduced the time for climatic "recovery" between each cycle, thereby providing a mechanism for the buildup of large terrestrial ice sheets. Thus, a combination of factors at different time scales within a nonlinear framework may be responsible for the changes leading to the NHG.

References and Notes

1. L. J. Lourens and F. J. Hilgen, *Quat. Int.* **40**, 43 (1997).
2. M. E. Raymo, D. Hodell, E. Jansen, *Paleoceanography* **7**, 645 (1992).
3. G. H. Haug and R. Tiedemann, *Nature* **393**, 673 (1998).
4. X. S. Li *et al.*, *Geophys. Res. Lett.* **25**, 915 (1998).
5. W. F. Ruddimann and J. E. Kutzbach, *J. Geophys. Res.* **94**, 18409 (1989).
6. M. E. Raymo, W. F. Ruddimann, P. N. Froelich, *Geology* **16**, 649 (1988).
7. M. A. Maslin, X. S. Li, M. F. Loutre, A. Berger, *Quat. Sci. Rev.* **17**, 411 (1998).
8. K. J. Willis, A. Kleczkowski, S. J. Crowhurst, *Nature* **397**, 685 (1999).
9. C. Ravasz, *Annu. Rep. Hung. State Geol. Inst. 1974* (1974), p. 221.
10. M. Hajós, *Annu. Rep. Hung. State Geol. Inst. 1988* (1989), p. 5.
11. N. J. Shackleton, M. A. Hall, D. Pate, in *Proceedings of the Ocean Drilling Program, Scientific Results*, N. G. Pisias, T. R. Janecek, A. Palmer-Julson, T. H. van Andel, Eds. (Ocean Drilling Program, College Station, TX, 1995), vol. 138, pp. 337–355.
12. M. A. Maslin, G. H. Haug, M. Sarnthein, R. Tiedemann, *Geol. Rundsch.* **85**, 452 (1996).
13. G. Kukla, *Boreas* **1**, 63 (1972).
14. J. Laskar, F. Joutel, F. Boudin, *Astron. Astrophys.* **270**, 522 (1993).
15. T. K. Hagelberg, G. Bond, P. deMenocal, *Paleoceanography* **9**, 545 (1994).
16. A. Berger and M. F. Loutre, *Science* **278**, 1476 (1997).
17. D. B. Percival and A. T. Walden, *Spectral Analysis for Physical Applications* (Cambridge Univ. Press, Cambridge, 1993).

18. This work was supported by a Royal Society University Research Fellowship (K.J.W.), a King's College Senior Research Fellowship (A.K.), Biotechnology and Biological Sciences Research Council (K.M.B. and C.A.G.), a Royal Society Leverhulme Trust Senior Research Fellowship (C.A.G.), and St. Hugh's College Oxford Higher Studies Fund (payment for color of Fig. 1), which we gratefully acknowledge.

4 January 1999; accepted 7 June 1999

Superradiant Rayleigh Scattering from a Bose-Einstein Condensate

S. Inouye,* A. P. Chikkatur, D. M. Stamper-Kurn, J. Stenger, D. E. Pritchard, W. Ketterle

Rayleigh scattering off a Bose-Einstein condensate was studied. Exposing an elongated condensate to a single off-resonant laser beam resulted in the observation of highly directional scattering of light and atoms. This collective light scattering is caused by the coherent center-of-mass motion of the atoms in the condensate. A directional beam of recoiling atoms was built up by matter wave amplification.

Rayleigh scattering, the scattering of a photon off an atom, is the most elementary process involving atoms and light. It is responsible for the index of refraction of gases, the blue sky, and resonance fluorescence. This process can be divided into absorption of a photon and subsequent spontaneous emission. Photon scattering imparts a recoil momentum to the atom. Because of the random nature of spontaneous emission, the direction of the recoil is random, leading to momentum diffusion and heating of the atomic motion.

With the realization of Bose-Einstein condensation (BEC) (*1*), it is now possible to study the interactions of coherent light with an ensemble of atoms in a single quantum state. The high degree of spatial and temporal coherence of a condensate was confirmed in several experiments (*2*, *3*). This raises the important question of whether the coherent external motion of the atoms can alter the interactions between atoms and light. Here we show that the long coherence time of a Bose-Einstein condensate introduces strong correlations between successive Rayleigh scattering events. The scattering of photons leaves an imprint in the condensate in the form of long-lived excitations that provide a positive feedback and lead to directional Rayleigh scattering.

The gain mechanism for Rayleigh scattering from a condensate can be derived semiclassically. When a condensate of N_0 atoms is exposed to a laser beam with wave vector $\mathbf{k}_0$ and scatters a photon with wave vector $\mathbf{k}_i$, an atom [or quasi-particle, also called momentum side mode in (*4*)] with recoil momentum $\hbar\mathbf{K}_j = \hbar(\mathbf{k}_0 - \mathbf{k}_i)$, where $\hbar$ is Planck's constant divided by 2π, is generated. Because light propagates at a velocity about 10 orders of magnitude greater than the atomic recoil velocity (3 cm/s for sodium), the recoiling atoms remain within the volume of the condensate long after the photons have left and affect subsequent scattering events. They interfere with the condensate at rest to form a moving matter wave grating of wave vector $\mathbf{K}_j$, which diffracts the laser beam into the phase-matching direction $\mathbf{k}_i$ ($= \mathbf{k}_0 - \mathbf{K}_j$). This diffraction is a self-amplifying process because every diffracted photon creates another recoiling atom that increases the amplitude of the matter wave grating.

When N_j recoiling atoms with momentum $\hbar\mathbf{K}_j$ interfere with N_0 condensate atoms at rest, the density modulation comprises $N_{\mathrm{mod}} = 2\sqrt{N_0 N_j}$ atoms. The light scattered by these atoms interferes constructively in the phase-matching direction with a total power P of

$$P = \hbar\omega f_j R \frac{N_{\mathrm{mod}}^2}{4} \quad (1)$$

$$f_j = \frac{\sin^2\theta_j}{8\pi/3}\Omega_j \quad (2)$$

Here, R is the rate for single-atom Rayleigh scattering, which is proportional to the laser intensity, and ω is the frequency of the radiation. The angular term in Eq. 2 reflects the dipolar emission pattern with θ_j being the angle between the polarization of the incident light and the direction of emission. Because of the finite size of the sample, the phase-matching condition is fulfilled over the solid angle $\Omega_j \sim \lambda^2/A$, where A is the cross-sectional area of the condensate perpendicular to the direction of the light emission and λ is the optical wavelength. More rigorously, Ω_j is given by the usual phase-matching integral for superradiance in extended samples (*5*):

$$\Omega_j = \int d\Omega(\mathbf{k}) \left| \int \tilde{\rho}(\mathbf{r}) e^{i(\mathbf{k}_i - \mathbf{k})\cdot\mathbf{r}} d\mathbf{r} \right|^2 \quad (3)$$

where $|\mathbf{k}| = |\mathbf{k}_i|$ and $\tilde{\rho}(\mathbf{r})$ is the normalized spatial density distribution in the condensate ($\int \tilde{\rho}(\mathbf{r})\, d\mathbf{r} = 1$).

Because each scattered photon creates a

Department of Physics and Research Laboratory of Electronics, Massachusetts Institute of Technology, Cambridge, MA 02139, USA.

*To whom correspondence should be addressed. E-mail: sinouye@mit.edu

recoiling atom, we obtain the growth rate for N_j from $P/\hbar\omega$:

$$\dot{N}_j = G_j N_j \quad (4)$$

This equation predicts exponential growth of N_j with the small-signal gain $G_j = RN_0 f_j \sim R \sin^2 \theta_j D_j$, where $D_j \sim \rho_0 \lambda^2 l_j$ is the resonant optical density for a condensate with an atomic density ρ_0 and a length l_j along the axis of emission. Therefore, for an anisotropic Bose condensate, the gain is largest when the light is emitted along its longest axis [the "end-fire mode" (*6*)]. Equation 4 is valid in the absence of decoherence and predicts the buildup of highly anisotropic Rayleigh scattering from a nonspherical sample of atoms.

For the experimental study of directional Rayleigh scattering, elongated Bose-Einstein condensates were prepared in a magnetic trap (*7*). The trapped condensates were about 20 μm in diameter d and 200 μm in length l and contained several million sodium atoms in the $F = 1$ hyperfine ground state. The condensate was exposed to a single off-resonant laser pulse that was red-detuned by 1.7 GHz from the $3S_{1/2}$, $F = 1 \rightarrow 3P_{3/2}$, $F = 0,1,2$ transition. The beam had a diameter of a few millimeters, propagated at an angle of 45° to the vertical axis, and intersected the elongated condensate perpendicular to its long axis (Fig. 1A). Typical laser intensities were between 1 and 100 mW/cm^2, corresponding to Rayleigh scattering rates of 4.5×10^1 to 4.5×10^3 s^{-1} and the pulse duration between 10 and 800 μs. To probe the momentum distribution of scattered atoms, we suddenly turned off the magnetic trap immediately after the light pulse and imaged the ballistically expanding cloud after 20- to 50-ms time of flight using resonant probe light propagating vertically onto a charge-coupled device (CCD) camera.

The momentum distributions of atoms after light scattering (Fig. 1B, to G) showed a marked dependence on the polarization of the incident laser beam. For polarization parallel to the long axis of the elongated condensate ($\theta_j = 0$), light emission into the end-fire mode was suppressed, and the distribution of atoms followed the dipolar pattern of normal Rayleigh scattering. For perpendicular polarization ($\theta_j = \pi/2$), photons were predominantly emitted along the long axis of the condensate, and the recoiling atoms appeared as highly directional beams propagating at an angle of 45° with respect to this axis (*8*).

A fully quantum-mechanical treatment reproduces the semiclassical result (Eq. 4) except that N_j is replaced by $N_j + 1$:

$$\dot{N}_j = RN_0 \frac{\sin^2\theta_j}{8\pi/3} \Omega_j (N_j + 1) \quad (5)$$

Equation 5 now describes both normal Rayleigh scattering at a constant total rate $\Sigma\dot{N}_j = RN_0$ when $N_j \ll 1$ and exponential gain of the jth recoil mode once N_j becomes nonnegligible. Initially, the angular distribution of the scattered light follows the single-atom spontaneous (dipolar) emission pattern but can become highly anisotropic when stimulation by the atomic field becomes important (*9*, *10*).

This phenomenon is analogous to the superradiance discussed by Dicke (*6*). He showed that the optical emission of incoherently excited atoms can be highly directional. The key feature of superradiance (or superfluorescence) (*11*) is that spontaneous emission is not a single-atom process but a collective process of all atoms, leaving the atoms in a coherent superposition of ground and excited states (*12*). The condensate at rest "pumped" by the off-resonant laser corresponds to the electronically excited state in the Dicke case. It can decay by a spontaneous Raman process to a state with photon recoil (corresponding to the ground state). The rate of superradiant emission in Dicke's treatment is proportional to the square of an oscillating macroscopic dipole moment. In the present case, the radiated intensity is proportional to the square of the contrast of the matter wave interference pattern between the condensate and the recoiling atoms.

A characteristic feature of superradiance is an accelerated decay of the initial state. In our experiment, normal exponential decay and the superradiant decay could be directly compared by tracing the number of atoms remaining in the condensate at rest after exposure to light of different polarizations. For parallel polarization, we observed a simple exponential decay with the expected Rayleigh scattering rate (Fig. 2). For perpendicular polarization, the end-fire mode was active, and the condensate decayed nonexponentially with a strongly accelerated superradiant rate.

To verify the directional emission of light, we observed the scattered light by directing it

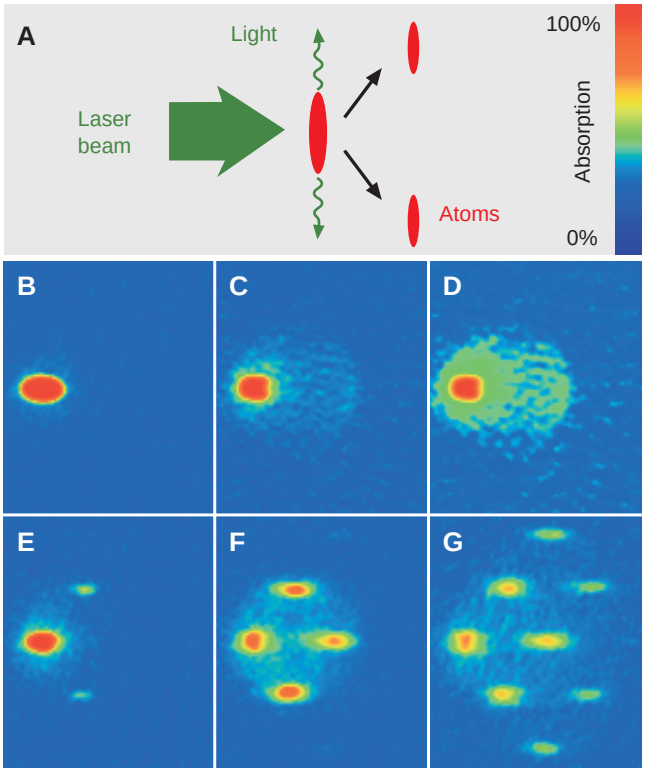

Fig. 1. Observation of superradiant Rayleigh scattering. (**A**) An elongated condensate is illuminated with a single off-resonant laser beam. Collective scattering leads to photons scattered predominantly along the axial direction and atoms at 45°. (**B** to **G**) Absorption images after 20-ms time of flight show the atomic momentum distribution after their exposure to a laser pulse of variable duration. When the polarization was parallel to the long axis, superradiance was suppressed, and normal Rayleigh scattering was observed (B to D). For perpendicular polarization, directional superradiant scattering of atoms was observed (E to G) and evolved to repeated scattering for longer laser pulses (F and G). The pulse durations were 25 (B), 100 (C and D), 35 (E), 75 (F), and 100 (G) μs. The field of view of each image is 2.8 mm by 3.3 mm. The scattering angle appears larger than 45° because of the angle of observation. All images use the same color scale except for (D), which enhances the small signal of Rayleigh scattered atoms in (C).

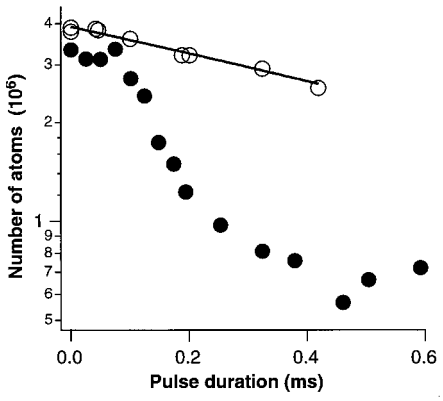

Fig. 2. The decay of atoms in the condensate at rest showed the normal exponential decay for parallel polarization (○) and faster superradiant decay for perpendicular polarization (●). The laser intensities (13 mW/cm^2) and oscillator strengths were equal in both cases.

onto a CCD camera (Fig. 3A). The camera was positioned out of focus of the imaging system, so that the images represent the angular distribution of photons emitted around the axial direction. The images consisted of bright spots with angular widths equal to the diffraction limit for a source with a diameter of ~14 μm. Typical images showed more than one such spot, and their pattern changed randomly under the same experimental conditions. The observation of a few spots is consistent with a Fresnel number $F = \pi d^2/4l\lambda$ slightly larger than 1, implying that the geometric angle d/l is larger than the diffraction angle λ/d. $F > 1$ leads to multimode superradiance (*11*) because there is now more than one end-fire mode.

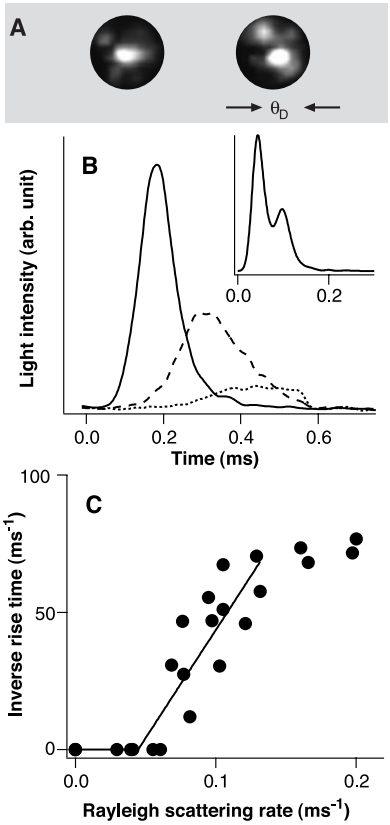

Fig. 3. Observation of directional emission of light. (**A**) The angular pattern of the emitted light along the axial direction showed a few bright spots with an angular width θ_D ($1/e^2$ diameter) of 107 ± 20 mrad, corresponding to the diffraction-limited angle of an object of ~14 μm in diameter. The images were integrated over the entire duration of the light pulse. (**B**) The temporal evolution of the light intensity showed a strong initial increase characteristic of a stimulated process. For higher laser power, the pulse was shorter and more intense. The laser intensities were 3.8 (solid line), 2.4 (dashed line), and 1.4 (dotted line) mW/cm^2, and the duration was 550 μs. The inset shows a double peak in the temporal signal when the laser intensity was about 15 mW/cm^2, which was above the threshold for sequential superradiant scattering. The photomultiplier recorded the light over an angle of 200 mrad around the axial direction. (**C**) The dependence of the inverse initial rise time on the Rayleigh scattering rate shows a threshold for the stimulated process. The solid curve is a straight-line fit.

By replacing the camera with a photomultiplier, a time-resolved measurement of the scattered light intensity was obtained (Fig. 3B). Simple Rayleigh scattering would give a constant signal during the square-shaped laser pulse. Instead, we observed a fast rise and a subsequent decay consistent with a stimulated process.

Measurements at variable laser intensities showed a threshold for the onset of superradiance and a shorter rise time for higher laser intensities. This behavior can be accounted for by adding a loss term L_j in Eq. 4:

$$\dot{N}_j = (G_j - L_j) N_j \qquad (6)$$

We determined the exponential rate $(G_j - L_j)$ by fitting the initial rise in the light intensity. At early times, the depletion of the condensate is negligible and G_j and L_j are constants. The inverse rise time $\dot{N}/N$ versus the Rayleigh scattering rate R, which was measured by "switching off" the superradiance by changing to parallel polarization, is shown in Fig. 3C. The slope gives G_j/R, and the offset determines the loss L_j. The agreement between the calculated value for $G_j/R \sim 890$ (with $\Omega_j \sim 1.9 \times 10^{-4}$ and $N_0 = 4.7 \times 10^6$) and the result of the simple linear fit (790) is better than the uncertainty in the Rayleigh scattering rate (40%). The offset in Fig. 3C determines the threshold for superradiance and yields $1/L_j = 35$ μs.

The rate of decoherence L_j for the superradiance indicates the decay of the matter wave interference. This decoherence has been studied separately by stimulated Rayleigh scattering (or Bragg spectroscopy) (*3*), where the linewidth of the Bragg resonance resulted from Doppler and mean-field broadening. The observed full width at half-maximum of about 5 kHz yields a decoherence time of 32 μs, in good agreement with the value shown above (*13*, *14*).

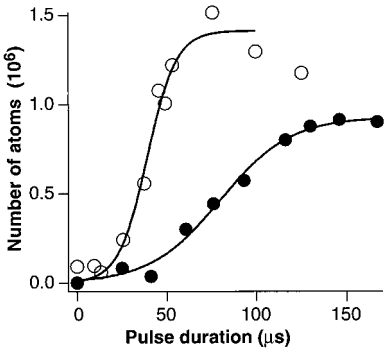

Fig. 4. Observation of "matter wave amplification." Shown is the number of atoms in one of the superradiant peaks versus duration of the laser pulse. An intense atomic pulse was formed by amplification of spontaneous scattering. The initial number of atoms in the condensate at rest was 2×10^7, and the laser intensities were about 25 (●) and 45 (○) mW/cm^2. The solid lines are guides to the eye.

For higher laser powers, a distinct change in both the momentum pattern of the atoms (Fig. 1, F and G) and the photomultiplier traces (Fig. 3B) was observed. The atomic pattern showed additional momentum peaks that can be explained as a sequential scattering process in which atoms in the initial momentum peak undergo further superradiant scattering (*15*). These processes are time-delayed with respect to the primary process and showed up as a second peak in the time-resolved photomultiplier traces (Fig. 3B). This "cascade" of superradiant scattering processes does not exist in the two-level superradiance systems studied so far.

Superradiance is based on the coherence of the emitting system, but it does not require quantum degeneracy. The condition for superradiance is that the gain exceed the losses or that the superradiant decay time be shorter than any decoherence time (*11*). Above the BEC transition temperature T_c, thermal Doppler broadening results in a 30 times shorter decoherence time than for a condensate. Furthermore, the larger size of the thermal cloud reduces the solid angle Ω_j and therefore the gain by a factor of 10. Therefore, the threshold for superradiance in a thermal cloud is several orders of magnitude higher than for a condensate. No signs of superradiant scattering were observed above T_c; rather, the sudden appearance of superradiant emission was a sensitive indicator for reaching the phase transition.

The rise of the number of atoms in the superradiant peak (Fig. 4) can be regarded as single-pass matter wave amplification. Recently, Law and Bigelow considered such an amplifier formed by passing input atoms through a condensate (*16*). The condensate atoms are transferred into the input atomic mode by bosonic stimulation, assisted by spontaneously scattered photons from a coupling laser that ensures momentum conservation and irreversibility of the gain process. Our experiment realized this geometry except for the fact that the input atoms were created spontaneously. The observed peak of recoiling atoms can thus be regarded as amplified vacuum fluctuations.

An atom cloud with a small excited state admixture can act as a gain medium for both matter waves and light, and we have observed the matter wave amplification. If the emitted light is allowed to build up in a cavity, an optical laser is realized (*17*). Similarly, the buildup of the matter wave field in an atom cavity can lead to an atom laser (*18*).

In conclusion, we have studied the interaction between coherent light and coherent atoms. The long coherence time of a Bose-

Einstein condensate gave rise to superradiance based on coherent external motion. The extremely low threshold in light intensity ($\sim$ 1 mW/cm^2 for our conditions) should be taken into account in BEC experiments that use optical probing and manipulation with off-resonant light. The simultaneous superradiant emission of light and atoms emphasizes the symmetry between atom lasers and optical lasers.

References and Notes

1. M. H. Anderson, J. R. Ensher, M. R. Matthews, C. E. Wieman, E. A. Cornell, *Science* **269**, 198 (1995); K. B. Davis *et al.*, *Phys. Rev. Lett.* **75**, 3969 (1995); C. C. Bradley, C. A. Sackett, R. G. Hulet, *ibid.* **78**, 985 (1997); D. G. Fried *et al.*, *ibid.* **81**, 3811 (1998).
2. M. R. Andrews *et al.*, *Science* **275**, 637 (1997); D. S. Hall, M. R. Matthews, C. E. Wieman, E. A. Cornell, *Phys. Rev. Lett.* **81**, 1543 (1998); B. P. Anderson and M. A. Kasevich, *Science* **282**, 1686 (1998).
3. J. Stenger *et al.*, *Phys. Rev. Lett.* **82**, 4569 (1999).
4. M. G. Moore and P. Meystre, *Phys. Rev. A* **59**, R1754 (1999).
5. N. E. Rehler and J. H. Eberly, *ibid.* **3**, 1735 (1971).
6. R. H. Dicke, in *Proceedings of the Third International Congress on Quantum Electronics*, P. Grivet and N. Bloembergen, Eds. (Columbia Univ. Press, New York, 1964), pp. 35–54.
7. M.-O. Mewes *et al.*, *Phys. Rev. Lett.* **77**, 416 (1996).
8. One can emphasize the symmetry of the atomic and optical fields by describing the process in the moving frame of the excited atoms that have absorbed one laser photon. Because the total momentum is zero in this frame, photons and atoms are emitted into opposite directions, preferentially along the long axis of the elongated cloud. Transforming back into the laboratory frame results in preferential emission of light still along the long axis but of atoms at 45°.
9. H.-J. Miesner *et al.*, *Science*, **279**, 1005 (1998).
10. The probability for reabsorption of scattered light was less than 3% and could be neglected. Optical amplification is accounted for by treating all the atoms as a single quantum mechanical system.
11. N. Skribanowitz, I. P. Herman, J. C. MacGillivray, M. S. Feld, *Phys. Rev. Lett.* **30**, 309 (1973); R. Bonifacio and L. A. Lugiato, *Phys. Rev. A* **11**, 1507 (1975); Q. H. F. Vrehen and H. M. Gibbs, in *Topics in Current Physics 27*, R. Bonifacio, Ed. (Springer-Verlag, Berlin, 1982), pp. 111–147; M. Gross and S. Haroche, *Phys. Rep.* **93**, 301 (1982).
12. R. H. Dicke, *Phys. Rev.* **93**, 99 (1954).
13. In (*3*), the recoiling atoms propagated perpendicular to the long axis of the condensate. The "finite size" contribution to the Doppler broadening was therefore twice that of the present geometry.
14. Elastic collisions at a maximum rate of $\sim$2 kHz do not contribute substantially to L_j, although they reduce the number of atoms in the superradiant peak by $\sim$50%.
15. Stimulated Raman scattering and four-wave mixing between matter waves [see L. Deng *et al.*, *Nature* **398**, 218 (1999)] may couple the different recoil modes and further affect the momentum distribution.
16. C. K. Law and N. P. Bigelow, *Phys. Rev. A* **58**, 4791 (1998).
17. This is called the coherent atomic recoil laser. See R. Bonifacio and L. De Salvo, *Nucl. Instrum. Methods Phys. Res. A* **341**, 360 (1994); M. G. Moore and P. Meystre, *Phys. Rev. A* **58**, 3248 (1998); P. R. Berman, *ibid.* **59**, 585 (1999); M. G. Moore, O. Zobay, P. Meystre, http://xxx.lanl.gov/abs/cond-mat/9902293.
18. M. Olshanii, Y. Castin, J. Dalibard, in *Proceedings of the XII Conference on Laser Spectroscopy*, M. Inguscio, M. Allegrini, A. Sasso, Eds. (World Scientific, New York, 1995), pp. 7–12; H. M. Wiseman and M. J. Collett, *Phys. Lett. A* **202**, 246 (1995); U. Janicke and M. Wilkens, in *Topics on Ultracold Atoms and BEC 7*, K. Burnett, Ed. (Optical Society of America, Washington, DC, 1997), pp. 38–47.

19. We thank C. E. Kuklewicz for experimental assistance, D. A. Kokorowski for critical reading of the manuscript, and H. M. Gibbs, P. Meystre, J. H. Eberly, E. M. Wright, and M. S. Feld for helpful discussions. This work was supported by the Office of Naval Research, NSF, Joint Services Electronics Program (Army Research Office), NASA, and the David and Lucile Packard Foundation. A.P.C acknowledges support from NSF, D.M.S.-K. from the Joint Services Electronics Program Graduate Fellowship Program, and J.S. from the Alexander von Humboldt–Foundation.

27 April 1999; accepted 28 June 1999

The U.S. Carbon Budget: Contributions from Land-Use Change

R. A. Houghton,* J. L. Hackler, K. T. Lawrence

The rates at which lands in the United States were cleared for agriculture, abandoned, harvested for wood, and burned were reconstructed from historical data for the period 1700–1990 and used in a terrestrial carbon model to calculate annual changes in the amount of carbon stored in terrestrial ecosystems, including wood products. Changes in land use released 27 ± 6 petagrams of carbon to the atmosphere before 1945 and accumulated 2 ± 2 petagrams of carbon after 1945, largely as a result of fire suppression and forest growth on abandoned farmlands. During the 1980s, the net flux of carbon attributable to land management offset 10 to 30 percent of U.S. fossil fuel emissions.

The rate at which carbon is accumulating in terrestrial ecosystems in the United States is uncertain, as are the mechanisms responsible for the current sink. Estimates based on measured changes in wood volumes (forest inventories) (*1*–*3*) range between 0.079 and 0.280 petagrams of carbon per year (Pg C year^{-1}). An estimate, based on atmospheric and oceanic data and models, and including southern Canada, calculated a sink of 1.7 ± 0.5 Pg C year^{-1} (*4*). Neither of these approaches identifies the mechanisms responsible for the sink (*5*). In contrast, although the changes in carbon associated with land-use change do not define the total net flux of carbon between land and atmosphere, they represent the portion of the flux that can be attributed to direct human activity, and it is this portion that is addressed by the United Nations Framework Convention on Climate Change and by the Kyoto Protocol. In this report, we estimate the annual flux of carbon in the United States attributable to changes in land use.

Our approach is based on two types of information: rates of land-use change and changes per hectare in carbon that follow a change in land use. We considered the conversion of natural ecosystems to croplands (cultivated) and pastures (not cultivated), the abandonment of croplands and pastures, harvest of industrial wood and fuel wood, and fire management, that is, the area annually burned by wildfires. Rates of agricultural clearing and abandonment and rates of wood harvest were obtained directly from the U.S. Department of Agriculture (USDA) for the period since 1945 (*6*) and largely from the U.S. Bureau of Census (*7*) for the period between 1700 and 1945. Areas burned each year were obtained from wildfire statistics of the U.S. Forest Service (*8*) for the period after 1930 and from pre-European burning rates (*9*) modified by settlement and logging practices for the years 1700–1930 (*10*). A more detailed description of the data, sources, and assumptions can be found elsewhere (*11*, *12*).

We divided the United States into seven geographic regions (each region including two to five natural ecosystems) for a total of 13 different ecosystems, not including croplands and pastures. The areas and carbon stocks of ecosystems in 1700 were determined from both natural areas (*13*) and current ecosystems (*14*). The fractions of vegetation left alive, killed, and burned as a result of human activity and fire were defined for each type of land use and ecosystem. The efficiency of industrial wood harvest increased through time, so that more wood was removed per hectare and less left as slash (dead vegetation) (*15*, *16*). Rates of forest growth after harvest, fire, and agricultural abandonment and rates of decay of organic matter for each ecosystem were obtained from the ecological literature (*17*). Changes in soil carbon included only the losses that resulted from cultivation and the reaccumulations that followed abandonment of cultivated land. These per hectare rates of carbon loss and accumulation after changes in land

Woods Hole Research Center, Post Office Box 296, Woods Hole, MA 02543, USA.

*To whom correspondence should be addressed. E-mail: rhoughton@whrc.org